

Boosting Convolution with Efficient MLP-Permutation for Volumetric Medical Image Segmentation

Yi Lin, Xiao Fang, Dong Zhang, Kwang-Ting Cheng *Fellow, IEEE*, Hao Chen*, *Senior Member, IEEE*

Abstract—Recently, the advent of vision Transformer (ViT) has brought substantial advancements in 3D dataset benchmarks, particularly in 3D volumetric medical image segmentation (Vol-MedSeg). Concurrently, multi-layer perceptron (MLP) network has regained popularity among researchers due to their comparable results to ViT, albeit with the exclusion of the resource-intensive self-attention module. In this work, we propose a novel permutable hybrid network for Vol-MedSeg, named PHNet, which capitalizes on the strengths of both convolution neural networks (CNNs) and MLP. PHNet addresses the intrinsic isotropy problem of 3D volumetric data by employing a combination of 2D and 3D CNNs to extract local features. Besides, we propose an efficient multi-layer permute perceptron (MLPP) module that captures long-range dependence while preserving positional information. This is achieved through an axis decomposition operation that permutes the input tensor along different axes, thereby enabling the separate encoding of the positional information. Furthermore, MLPP tackles the resolution sensitivity issue of MLP in Vol-MedSeg with a token segmentation operation, which divides the feature into smaller tokens and processes them individually. Extensive experimental results validate that PHNet outperforms the state-of-the-art methods with lower computational costs on the widely-used yet challenging COVID-19-20 and Synapse benchmarks. The ablation study also demonstrates the effectiveness of PHNet in harnessing the strengths of both CNNs and MLP¹.

I. INTRODUCTION

Computer-aided diagnosis (CAD) systems have gained popularity in the healthcare sector, assisting radiologists in diagnosing and treating patients. Convolution neural networks (CNNs) have shown remarkable advancements, improving the performance of CAD, particularly in medical image segmentation (MedSeg) [1-3]. Over the past decades, substantial research efforts have focused on developing efficient and robust MedSeg methodologies. One of the most popular architectures for this task is UNet [4], which employs an encoder-decoder structure and skip connections to reserve both contextual and semantic information. Building upon the success of UNet, numerous variants have been proposed with various convolution-based blocks and different skip connections strategies, including ResUNet [5], Y-Net [6], and V-Net [7], etc.

Recently, Transformers with attention mechanism have shown promising superiority in the realm of natural language processing [8]. Subsequent studies, such as ViT [9] and DeiT [10], have demonstrated remarkable capabilities in achieving state-of-the-art performance on versatile computer vision tasks. Given the notable strides of Transformers in natural image recognition tasks, researchers have investigated

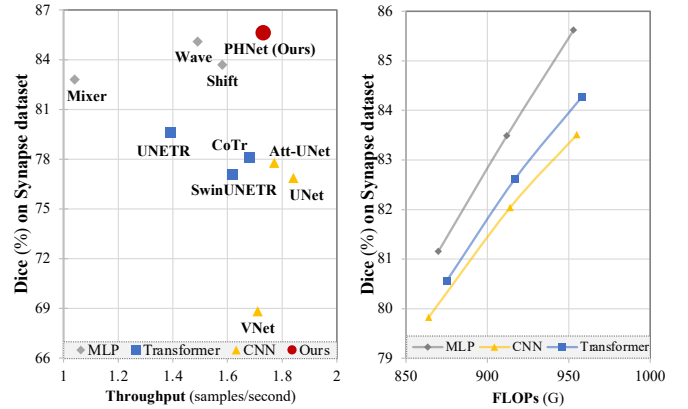


Fig. 1. Left: Performance v.s. throughput of PHNet and other SOTA methods. Right: performance v.s. FLOPs of CNN, Transformers, and MLP, in different model capacity.

the effectiveness of these neural networks for MedSeg. To name a few, TransUNet [3] proposed to employ a Transformer in the bottleneck of a UNet architecture for global information communication. Similarly, UNETR [11], CoTr [12], and SwinUNet [1] designed a hierarchical fusion of Transformer and CNNs architecture.

Despite the developments in MedSeg domain via Transformer methods, their heavy computational costs caused by the self-attention limit their practical application, particularly for 3D volumetric medical images, which necessitate a substantial number of forward and backward passes [13]. Consequently, multi-layer perceptron (MLP) has regained interest in the community, as it has demonstrated comparable performance with both CNNs and Transformers (in Figure 1), without requiring the heavy self-attention mechanism [14]. For instance, MLP-Mixer [14] enabled information communication by a series of MLPs, capturing long-range dependencies in the input data. However, the effectiveness of MLP in volumetric MedSeg remains understudied.

In this paper, we propose PHNet, a novel **Permutable Hybrid Network** that integrates the strengths of CNN and MLP for volumetric medical image segmentation. As illustrated in Figure 2, PHNet embodies an encoder-decoder paradigm. Notably, the encoder utilizes a 2.5D CNN structure that capitalizes on the inherent isotropy of medical images, while avoiding information loss in shallow layers by capturing the varying information density in different directions of volumetric medical images. In PHNet, we further propose MLPP, a Multi-Layer Permute Perceptron module that can maintain the positional information with the axial decomposition operation while integrating global interdependence

The first two authors contributed equally and asterisk indicates the corresponding author.

¹The code will be accessible to the public upon acceptance.

in a computationally-efficient manner. To enhance computational efficiency, token-group operation is introduced, which efficiently aggregates feature maps at a token level, reducing the number of computations required. PHNet is evaluated on two publicly available datasets, COVID-19 Lung CT Lesion Segmentation Challenge-2020 [15] and Synapse Multi-Organ Segmentation [16]. Extensive experimental results validate that PHNet achieves state-of-the-art performance on both datasets, surpassing the winner in MICCAI COVID-19-20 challenge.

II. RELATED WORK

A. CNN-Based Networks.

Since the groundbreaking introduction of the UNet [4], CNN-based networks have achieved state-of-the-art results on various 2D and 3D MedSeg tasks [17-20]. These methods use CNNs as the backbone to extract image features, and combine some elaborate tricks (*e.g.*, skip connection, multi-scale representation, feature interaction) for feature enhancement. Compared to 2D methods, 3D approaches directly utilize the full volumetric image represented by a sequence of 2D slices or modalities. Despite their success, CNN-based networks exhibit a constraint in effectively learning global context and long-range spatial dependencies, resulting in sub-optimal performance for challenging tasks.

B. Transformer-Based Networks.

Vision Transformers have been applied in MedSeg to establish long-range dependence and capture context information. For example, UNETR [11] leverages Transformer as the encoder to learn sequence representations, which captures the global multi-scale information. Due to high computational costs, many architectures have been proposed to reduce the cost. Peiris *et al.* introduces VT-UNet [21] that leverages a hierarchical vision Transformer which gradually decreases the resolution of features in Transformer layers and utilizes sub-sampled attention modules. Chen *et al.* proposes TransUNet [3] which uses CNN to efficiently extract local information and employs a Transformer to model global features. Tang *et al.* proposes SwinUNETR [22] that calculates the attention weight between different tokens in shifted local windows, reducing the computational cost from quadratic to linear complexity. However, the self-attention mechanism is still computationally expensive and relatively slow on GPUs.

C. MLP-Based Networks.

Acknowledging the substantial computational cost of attention blocks in Transformer, simple and efficient modules that consist of only MLPs are proposed. Notably, MLP-Mixer [14] uses token-mixing MLP and channel-mixing MLP to capture the relationship between tokens and channels, respectively. CycleMLP [23] introduces a hierarchical cycle fully connected layer to aggregate spatial context and improve performance. WaveMLP [24] represents each token as a wave function with amplitude and phase to dynamically aggregate features according to the semantic contents of input images. In MedSeg field, UNeXt [13] shifts tokens along vertical and horizontal

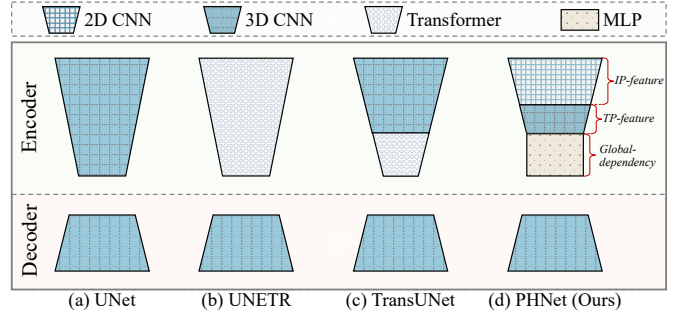


Fig. 2. Overview of the proposed PHNet.

directions to get an axial receptive field of 2D images to increase efficiency. However, the effects of MLPs in Vol-MedSeg remains unexplored. To the best of our knowledge, it is the first attempt to investigate the effectiveness of integrating CNNs and MLPs in Vol-MedSeg.

III. METHODOLOGY

PHNet adopts an encoder-decoder paradigm, as exemplified in Figure 2. The encoder consists of a 2.5D convolution module and an MLPP module. The 2.5D convolution is responsible for extracting local features, and the output feature maps are subsequently forwarded to MLPP to capture global features. The decoder processes the hierarchical features for prediction. In the following, we will detail each component.

A. 2.5D Convolution

Drawing upon previous research on bias in medical image analysis [25] and the anisotropic nature of volumetric medical images, we incorporate convolutional layers in the shallow layers of the encoder to extract local features. Volumetric images, such as CT and MRI scans, are often affected by anisotropic problems due to their thick-slice scanning [26], resulting in high in-plane (IP) resolution and low through-plane (TP) resolution [18, 20]. This discrepancy is particularly pronounced in COVID-19-20 [15], where the IP resolution is 0.74mm on average, while the TP resolution plunges to a mere 5mm. To mitigate this issue, we use 2D conv-blocks to capture the IP information until the feature is reformulated in approximately uniform resolution across all three axes: axial, coronal, and sagittal. Then, we apply 3D conv-blocks to handle the volumetric information. Each encoder layer consists of two residual convolution blocks, with each block comprising two sequential Convolution-Instance Normalization-Rectified Linear Unit (Conv-IN-ReLU) operations [27]. The residual addition takes place before the final ReLU activation.

B. Multi-Layer Permute Perceptron (MLPP)

Although CNNs are capable of modeling long-range dependencies through deep stacks of convolution layers, studies [13, 14, 28] have highlighted the superior ability of MLP-based networks to learn global context. Motivated by this, we design MLPP as depicted in Figure 3 to acquire global information in deep layers of the encoder. MLPP decomposes

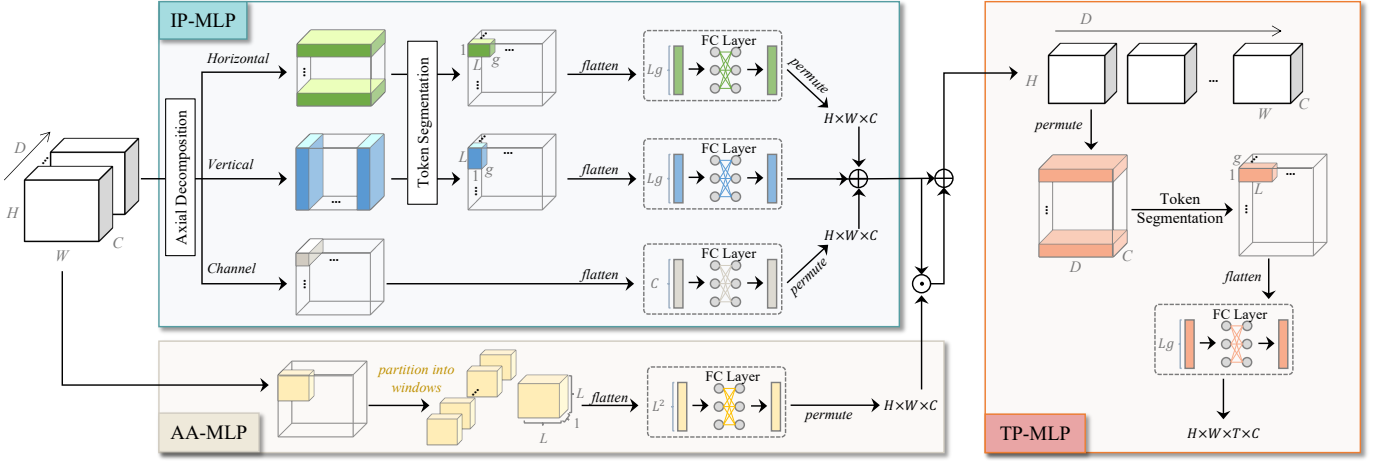


Fig. 3. Illustration of multi-layer permute perceptron (MLPP) module.

the training of IP feature and TP feature in sequential order. We denote these two blocks as **IP-MLP** and **TP-MLP**, respectively. To facilitate communication of cross-axis tokens, we further propose an auxiliary attention branch in IP-MLP, denoted as **AA-MLP**. We provide a PyTorch-style pseudo code of MLPP in the supplementary material.

1) **IP-MLP**.: Given one slice of input feature maps $\mathbf{X} \in \mathbb{R}^{H \times W \times C}$, conventional MLP-based methods [14, 29] typically flatten \mathbf{X} into a 1D vector, which loses the spatial information of the original conv-features [30] and results in large computational complexity which escalates quadratically with the size of \mathbf{X} . To this end, as depicted in Figure 3, we introduce an axial decomposition operation in triplet pathways that separately process \mathbf{X} in horizontal (W), vertical (H), and channel (C) axis. It is achieved by permuting dimensions of \mathbf{X} such that voxels within the same pathway across all channels are grouped, thus enabling the preservation of precise positional information along other axes when encoding information along one axis. It also reduces the computational complexity, which scales linearly with the size of \mathbf{X} .

To strike a balance between local feature and long-distance interactions, and alleviate image resolution sensitivity problem [31] wherein the MLP-based model is sensitive to the input resolution², we present a token segmentation operation that splits the feature vector into multiple tokens, which can be efficiently processed by the following fully-connected (FC) layers. We take the horizontal axis as an example. Instead of encoding the entire dimension, we split \mathbf{X} into non-overlapping segments along the horizontal direction. Each segment, denoted as $\mathbf{X}_i \in \mathbb{R}^{L \times C}$, where $i \in \{1, \dots, HW/L\}$, has a segment length of L . Similarly, we divide each \mathbf{X}_i into multiple non-overlapping groups along channel dimension, where each group has $g = C/L$ channels. This yields split segments, and each individual segment is $\mathbf{X}_i^k \in \mathbb{R}^{Lg}$, where $k \in \{1, \dots, C/g\}$. Next, we flatten each segment and map $\mathbb{R}^{Lg} \mapsto \mathbb{R}^{Lg}$ by an FC layer to transform each segment, producing \mathbf{Y}_i^k . To recover the original dimension, we permute all segments back to $\mathbf{Y}_W \in \mathbb{R}^{H \times W \times C}$. Similarly, we conduct the

same operations in the vertical pathway as above to permute tokens along the vertical direction, yielding \mathbf{Y}_H . To facilitate communication among groups along channel dimension, we design a parallel branch that contains an FC layer that maps $\mathbb{R}^C \mapsto \mathbb{R}^C$ to process each token individually, yielding \mathbf{Y}_C . Finally, we feed the element-wise summation of horizontal, vertical, and channel features into a new FC layer to attain the output, which can be formulated as:

$$\mathbf{Y}_{\text{IP}} = (\mathbf{Y}_H + \mathbf{Y}_W + \mathbf{Y}_C)\mathbf{W}, \quad (1)$$

where $\mathbf{W} \in \mathbb{R}^{C \times C}$ denotes an FC weight matrix.

2) **AA-MLP**.: The MLPP, despite its strengths, possesses two limitations that may have a negative impact on segmentation performance. First, the axial decomposition operation restricts direct interaction between tokens that are not in the same horizontal or vertical position. Second, the token segmentation operation would suffer from a smaller local reception field compared with the vanilla MLP [14]. To overcome these limitations, we design an auxiliary branch to enable intra-axis token communication, which serves as an attention mechanism via a lightweight yet effective MLP-like architecture. Specifically, given an input slice of feature maps $\mathbf{X} \in \mathbb{R}^{H \times W \times C}$, we partition \mathbf{X} into non-overlapping windows. We set window size to L and thus obtain $\mathbf{X}_i \in \mathbb{R}^{L \times L}$, where $i \in \{1, \dots, HWC/L^2\}$. Subsequently, we apply an FC matrix $\mathbf{W} \in \mathbb{R}^{L^2 \times L^2}$ to transform each window and get $\mathbf{Y}_i \in \mathbb{R}^{L \times L}$. The final attention map $\mathbf{Y}_A \in \mathbb{R}^{H \times W \times C}$ is obtained by permuting all windows back to the original dimension. Finally, the feature maps \mathbf{F}_{IP} of IP-MLP are obtained by performing residual attention [32] of \mathbf{Y}_{IP} and \mathbf{Y}_A as follows:

$$\mathbf{F}_{\text{IP}} = (1 + \mathbf{Y}_A) \odot \mathbf{Y}_{\text{IP}}, \quad (2)$$

where \odot denotes element-wise multiplication.

3) **TP-MLP**.: Upon obtaining the in-plane information from the IP-MLP module, we proceed to apply the TP-MLP module to capture the long-term through-plane features. Similarly, given input feature maps $\mathbf{F}_{\text{IP}} \in \mathbb{R}^{H \times W \times D \times C}$, we first split $\mathbf{X} = \mathbf{F}_{\text{IP}}$ along the depth dimension into non-overlapping segments with a segment length of L . We thus obtain $\mathbf{X}_i \in$

²Further discussion is provided in supplementary material.

$\mathbb{R}^{L \times C}$, where $i \in \{1, \dots, HWD/L\}$. Subsequently, we divide \mathbf{X} into several non-overlapping groups along the channel dimension, with each group containing $g = C/L$ channels. This results in $\mathbf{X}_i^k \in \mathbb{R}^{Lg}$, where $k \in \{1, \dots, C/g\}$. Subsequently, we flatten each segment and map $\mathbb{R}^{Lg} \mapsto \mathbb{R}^{Lg}$ by an FC layer, yielding \mathbf{Y}_i^k . Finally, we permute all segments $\mathbf{Y}_i^k \in \mathbb{R}^{Lg}$ back to the original dimension, yielding the output $\mathbf{F}_{TP} \in \mathbb{R}^{H \times W \times D \times C}$.

C. Decoder Network

The decoder in our proposed method utilizes a slim CNN architecture, employing transpose convolution to progressively upsample the feature maps to match the input image resolution. Within the decoder, we separate an isotropic 3D convolution with kernel size $3 \times 3 \times 3$ into a $3 \times 3 \times 1$ in-plane convolution and a $1 \times 1 \times 3$ through-plane convolution to efficiently fuse the feature [33]. We further include skip connections between the encoder and decoder, allowing for the preservation of low-level details.

IV. EXPERIMENTS

A. Datasets and Evaluation Metrics

We conduct experiments on two publicly available datasets: COVID-19-20 [15] and Synapse [16]. COVID-19-20 is comprised of 249 unenhanced chest CT scans, with 199 samples designated for training and 50 samples for testing. All samples are positive for SARS-CoV-2 RT-PCR. Synapse consists of 30 cases of CT scans, with 14, 4, and 12 cases designated for training, validation, and testing, respectively [1]. For COVID-19-20, we use the official evaluation metrics from the challenge [15], including Dice coefficient (Dice), Intersection over Union (IoU), Surface Dice coefficient (SD), Normalized Volume Difference (NVD), and Hausdorff Distance (HD). For Synapse, we follow [3] to adopt Dice and HD as evaluation metrics. The computational cost is measured with an input size of $192 \times 192 \times 48$ and a batch size of 1, in terms of FLOPS (G), Parameters (M), Peak Memory (G) and Throughput (samples/s). For details, please refer to [28].

B. Implementation Details

PHNet is implemented using PyTorch and MONAI [34] framework and trained on an NVIDIA RTX 3090 GPU. For COVID-19-20, all images are interpolated into the voxel spacing of $0.74 \times 0.74 \times 5.00\text{mm}^3$. Three sub-volumes of $224 \times 224 \times 28$ are sampled from each scan. We train PHNet for a total of 250 epochs on Synapse and 450 epochs on COVID-19-20. For all experiments we adopt the AdamW optimizer [35] with an initial learning rate $lr = 10^{-3} \times \frac{\text{batch_size}}{1024}$, as suggested by [28]. The objective function is the summation of Dice loss and cross-entropy loss. Except for the above, we follow baseline from [15] and [36] for the COVID-19-20 and Synapse datasets, respectively.

C. Comparisons with State-of-the-Arts

1) *Comparison methods.*: We compare the proposed PHNet with CNN-based, Transformer-based, MLP-based methods, and foundation model. We list the details below.

- *CNN-based methods*, including V-Net [7], UNet [4], nnUNet [36], and attention-UNet [37]. These architectures feature a hierarchical contracting path for context aggregation and a symmetric expanding path for resolution recovery and precise localization.
- *Transformer-based methods*, including ViT [9], UNETR [11], SwinUNETR [22], TransUNet [3], SwinUNet [1], CoTr [12], and CTO-Net [38]. These architectures can be classified into three categories: 1) classical Transformer (*i.e.*, ViT), 2) encoder-decoder framework with pure Transformer blocks (*i.e.*, SwinUNet), and 3) hybrid architectures with CNN and Transformer (*i.e.*, UNETR, SwinUNETR, TransUNet, CoTr, CTO-Net).
- *MLP-based methods*, including UNext [13], CycleMLP [23], MLP-Mixer (Mixer) [14], ShiftMLP (Shift) [39], and WaveMLP (Wave) [24]. We only replace the MLPP module in PHNet with these alternatives for a fair comparison.
- *SAMed* [40] is built upon SAM [41] which is a foundation model for semantic segmentation. SAMed retains the same architecture as SAM, which features a ViT-based encoder, a prompt module, and a mask decoder. SAMed applies the LoRA [42] finetuning strategy on target tasks.

2) *Quantitative comparisons.*: We begin by evaluating the performance of our method in multi-organ segmentation on Synapse [16] in Table I. Result shows that our method achieves the highest average Dice score of 85.62% and lowest HD of 11.75, outperforming the SOTA methods. Specifically, our method achieves 1.64% and 8.77% Dice improvements over nnUNet [36] and UNet [19], whose backbones are built upon 3D CNNs. Compared to top-performing competitors of Transformer-based CTO-Net [38], UNETR [11], MLP-based UNext [13], Wave [24], and SAMed [40], our method also achieves better performance with 4.52%, 6.05%, 18.55%, 0.53%, 3.74% Dice gains, respectively. These results conform to our argument that PHNet obtains satisfying segmentation performance through effective local-to-global modeling.

We further evaluate the performance on COVID-19-20 [15] and the official evaluation result is presented in Table II. Compared to CNN-based methods, our method attains the highest scores in all metrics. This suggests that CNN-based approaches have limitations in long-distance context fusion. Compared to Transformer-based methods, PHNet also achieves better performance, suggesting that our proposed hybrid structure design facilitates more adept feature learning. Compared to MLP-based methods, PHNet outperforms by a remarkable margin. This is partly because existing MLP-based methods are designed to segment on 2D slices which lose through-plane features, resulting in severe performance deterioration in challenging volumetric image segmentation tasks. The large performance gap between SAMed [40] and PHNet indicates the constrained generalization capacity of foundation models within specific segmentation tasks. Additionally, follow-

TABLE I
RESULT COMPARISONS WITH THE STATE-OF-THE-ART METHODS ON SYNAPSE [16].

	Methods	mDice \uparrow	HD \downarrow	Aorta	Gallb.	Kid(L)	Kid(R)	Liver	Panc.	Spleen	Stom.
CNN-based	UNet [4]	76.85	39.70	89.07	69.72	77.77	68.60	93.43	53.98	86.67	75.58
	V-Net [7]	68.81	-	75.34	51.87	77.10	80.75	87.84	40.05	80.56	56.98
	Attention-UNet [37]	77.77	36.02	89.55	68.88	77.98	71.11	93.57	58.04	87.30	75.75
	nnUNet [36]	83.98	12.56	<u>91.73</u>	66.22	<u>87.30</u>	84.41	<u>96.15</u>	76.04	94.81	75.20
Transformer-based	ViT [9]	71.29	32.87	73.73	55.13	75.80	72.20	91.51	45.99	81.99	73.95
	TransUNet [3]	77.48	31.69	87.23	63.13	81.87	77.02	94.08	55.86	85.08	75.62
	CoTr [12]	78.08	27.38	85.87	61.38	84.83	79.36	94.28	57.65	87.74	73.55
	UNETR [11]	79.57	23.87	89.99	60.56	85.66	<u>84.80</u>	94.46	59.25	87.81	73.99
	SwinUNETR [22]	77.09	34.21	88.73	60.07	78.10	80.99	93.81	51.97	89.72	73.29
	SwinUNet [1]	79.13	21.55	85.47	66.53	83.28	79.61	94.29	56.58	90.66	76.60
	CTO-Net [38]	81.10	18.75	87.72	66.44	84.49	81.77	94.88	62.74	90.60	80.20
MLP-based	Mixer [14]	82.80	21.12	87.40	67.16	85.37	83.96	95.16	70.53	94.53	78.25
	UNeXt [13]	67.07	40.47	76.43	51.64	74.54	67.94	91.11	34.95	79.20	60.70
	CycleMLP [23]	70.82	24.47	75.07	61.75	77.25	70.71	92.83	42.29	81.44	65.26
	Shift [39]	83.69	16.44	91.35	64.50	86.68	84.15	96.01	73.62	95.22	78.01
	Wave [24]	<u>85.09</u>	<u>12.49</u>	91.74	<u>72.48</u>	86.37	84.63	96.03	77.02	95.25	77.23
	SAMed [40]	81.88	20.64	87.77	69.11	80.45	79.95	94.80	72.17	88.72	82.06
	PHNet (Ours)	85.62	11.75	90.31	74.08	87.46	85.69	96.16	<u>76.94</u>	<u>95.23</u>	<u>79.11</u>

ing [15], we perform five-fold cross-validation and model ensemble using our proposed method. The result demonstrates that our method achieves the highest dice score of 77.18%, surpassing the performance of the top-12 solutions in this challenge³.

Additionally, our method is subjected to further evaluation on two other public datasets, namely the Liver Tumor Segmentation dataset (LiTS) [43] and the Medical Segmentation Decathlon (MSD) brain tumor segmentation (BraTS) [44] dataset. The details are presented in the supplementary material. Results show that our method outperforms other state-of-the-art methods on both datasets, demonstrating the credibility and wide-ranging applicability of our proposed method.

3) *Qualitative comparisons.*: Visual comparisons on Synapse [16] are shown in Figure 4. PHNet achieves the best visual segmentation results compared to nnUNet [36], TransUNet [3], UNeXt [13], and Mixer [14]. As shown in the first row, the comparison indicates that our method achieves a better segmentation where the under-segmentation of pancreas is observed in nnUNet, TransUNet, and UNeXt. Moreover, as shown in the second row, PHNet can accurately delineate boundaries between liver and stomach, while the over-segmentation of liver is observed in both UNeXt and Mixer. Similarly, PHNet delineates a more precise boundary between pancreas and stomach as shown in the last row. The primary

factor could be PHNet helps extract accurate contours by effective local-to-global modeling and aggregation of inter-axis and intra-axis token features. Overall, PHNet attains better segmentation results and mitigates the issues associated with under- and over-segmentation contours.

D. Ablation Study

We conduct ablation studies on Synapse to validate the effectiveness and efficiency of each component in our method. We use the same decoder architecture for all variations.

1) *Effectiveness of each components.*: To verify the effectiveness of core components in our approach, we increase each essential component gradually based on the vanilla MLP network (abbreviated as “baseline”), as shown in Table III. Compared with the baseline, the integration of axial decomposition yields a 1.49% enhancement in Dice and a noteworthy improvement in efficiency. This is due to positional information encoding and complexity reduction. There is an additional improvement of 0.65% Dice through decomposition into in-plane and through-plane features, which is attributed to the amplified learning capacity of the module as it contains distinct learning parameters for in-plane and through-plane features [45]. Furthermore, AA-MLP contributes to 0.68% performance gains with slightly increasing computational cost, and the whole framework achieves an 85.62% Dice score. This is because intra-axis token communication enables better learning representation from larger receptive field, as shown

³<https://covid-segmentation.grand-challenge.org/evaluation/challenge/leaderboard>

TABLE II
RESULT COMPARISONS WITH THE STATE-OF-THE-ART METHODS AND TOP-12 SOLUTIONS ON COVID-19-20 [15].

Methods		Dice \uparrow	IoU \uparrow	SD \uparrow	NVD \downarrow	HD \downarrow	Method	Dice \uparrow
CNN	UNet [19]	69.09	55.27	62.83	40.79	134.76	Rank 1	77.09
	nnUNet [36]	72.51	59.40	69.04	27.87	123.65	Rank 2	76.87
Transformer	TransUNet [3]	18.64	11.70	11.93	65.06	279.03	Rank 3	76.87
	CoTr [12]	59.63	45.65	52.97	44.57	172.78	Rank 4	76.78
	UNETR [11]	57.18	43.10	51.20	44.64	174.40	Rank 5	76.77
	SwinUNETR [22]	63.65	50.13	58.19	37.20	141.42	Rank 6	76.64
	SwinUNet [1]	32.82	22.08	20.71	67.62	221.46	Rank 7	76.47
MLP	Shift [39]	72.18	59.32	68.58	25.27	132.01	Rank 8	76.45
	Wave [24]	<u>74.08</u>	<u>60.92</u>	<u>70.76</u>	<u>22.12</u>	<u>120.59</u>	Rank 9	76.28
	UNeXt [13]	21.90	14.64	10.79	81.52	328.83	Rank 10	76.27
	CycleMLP [23]	27.53	17.91	15.55	79.67	228.07	Rank 11	76.27
SAMed [40]		15.43	09.52	7.66	96.36	2265.73	Rank 12	76.16
PHNet (Ours)		76.34	63.36	72.10	20.60	108.16	Ours	77.18

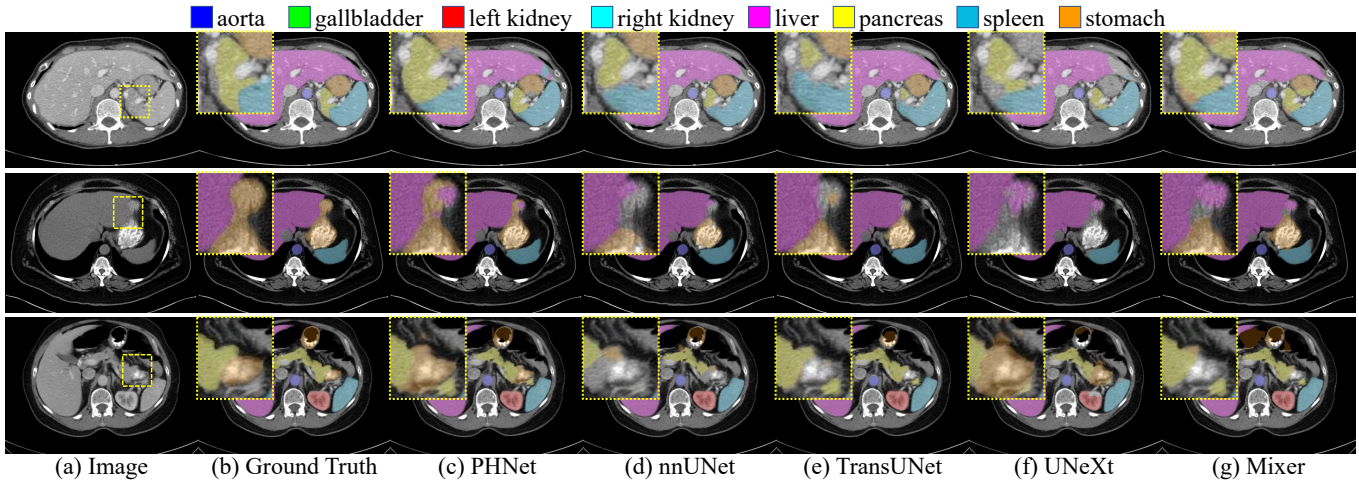


Fig. 4. Qualitative visualizations of different methods on the Synapse [16]. Regions of evident improvements are enlarged to show better details.

TABLE III

RESULT COMPARISONS WITH DIFFERENT EFFECTS OF EACH COMPONENT ON SYNAPSE [16]. “BASELINE” DENOTES THE VANILLA MLP NETWORK. “IP-” DENOTES THE PROPOSED AXIAL DECOMPOSITION OPERATION IN IP-MLP MODULE. “TP-” DENOTES THE PROPOSED OPERATION OF DECOMPOSITION OF IN-PLANE FEATURE AND THROUGH-PLANE FEATURE IN TP-MLP. “AA-” DENOTES OUR PROPOSED AA-MLP MODULE.

Baseline	IP-	TP-	AA-	Dice \uparrow	HD \downarrow	FLOPs	Thro.
✓				82.80	21.12	1249	1.04
✓	✓			84.29	19.05	938	1.73
✓		✓		83.39	19.66	971	1.62
✓	✓	✓		84.94	18.29	947	1.75
✓	✓	✓	✓	85.62	11.75	953	1.73

in Figure 5. A similar trend can be observed in the evaluation of HD metric. These results underscore the effectiveness of each component in our approach.

2) *Impact of segment length.*: In Figure 6(a), we investigate the impact of different segment lengths L in PHNet. Expressly, the segment length is set to various ratios of the width (W), *i.e.*, 1 , $\frac{1}{2}$, $\frac{1}{3}$, and $\frac{1}{4}$, respectively. With a larger segment length, long-range dependencies can be more effectively captured in deep layers. Conversely, smaller segment length implies fewer adjacent tokens are grouped, emphasizing more on local information. The best performance is achieved when $L = \frac{1}{2}W$, which provides a good balance between local information and long-range dependencies.

3) *Impact of MLP layers.*: In Figure 6(b), we study the influence of a different number of MLP layers K in our PHNet. Results show that the best performance is achieved when the number of MLP layers is 2. This observation may vary across datasets. Our method consistently outperforms the baseline method across different configurations of MLP layers,

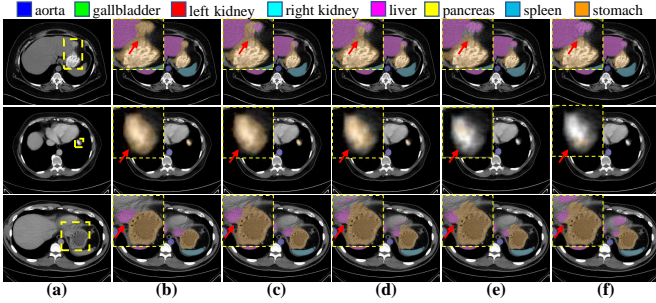


Fig. 5. Segmentation visualizations of ablation variations on Synapse [16], including (a) original image, (b) ground truth, predictions of (c) baseline + IP + TP + AA, (d) baseline + IP + TP, (e) baseline + IP, and (f) baseline. Regions of evident improvements are enlarged to show better details. Better viewed with zooming in.

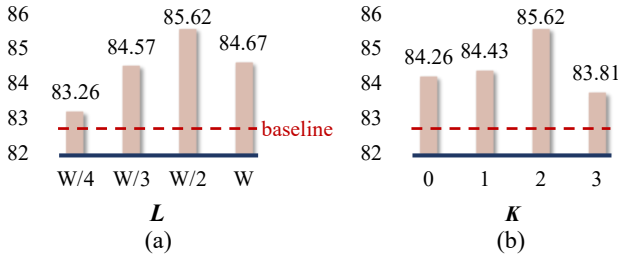


Fig. 6. Impact of (a) different segment length L ; (b) different number of MLP layers K on Synapse dataset.

affirming the robustness and stability of our method.

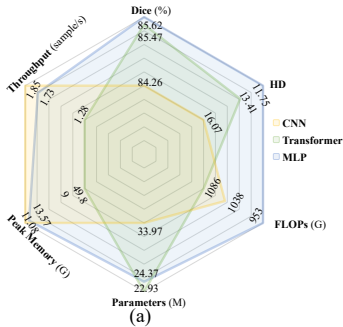


Fig. 7. (a) Comparisons between conventional architectures in terms of effectiveness and efficiency; (b) Comparison between architecture combinations in Dice (%).

E. Discussion

1) *Comparisons with conventional architectures.*: We conduct experiments to validate our analysis as shown in Fig. 7(a). Specifically, we replace the MLPP module with 3D CNN and Transformer blocks to assess their impact on efficiency and effectiveness. For the Transformer component, we opt for the advanced Swin Transformer [22] due to the promising performance and notable reduction in computational cost through the use of shift windows. Compared to CNN, our method achieves 1.36% improvement in Dice, indicating that our proposed MLPP module more effectively encodes the global information, leading to enhanced segmentation accuracy. Concerning computational efficiency, our method achieves a profile of

953G FLOPs, 24.37M parameters, 13.57G peak memory, and 1.73 samples/second throughput. These efficiency outcomes are comparable to those of 3D CNN, indicating that augment CNN performance while upholding efficiency. Although Transformer showcases competitive performance when configured with stacked blocks, our method shows significant superiority in terms of efficiency. This suggests that our MLPP is capable of capturing global information while eliminating the exhaustiveness of token comparison seen in self-attention. We also provide theoretical analysis for the computational cost in the supplementary material.

2) *Comparisons with architecture combinations.*: We further conduct a comprehensive experimental analysis of various combinations of CNN, Transformer and MLP in both shallow and deep layers of the encoder. As depicted in Figure 7(b), the combination of CNN in shallow layers and MLP in deep layers achieves the best performance with an 85.62% Dice score. This finding supports our argument that CNN excels in capturing local features, while MLP is more effective in modeling long-range dependencies. Interestingly, the inverse configuration, which employs MLP in shallow layers and CNN in deep layers, results in a significant decline in performance. This suggests that local information can be effectively extracted in shallow layers, while global information is better captured in deeper layers. We also observe that the performance of Transformer architectures is underwhelming, which may be due to their high model complexity leading to overfitting on small datasets.

V. CONCLUSION

This paper introduced a novel permutable hybrid network, PHNet, specifically designed for volumetric medical image segmentation. By integrating 2D CNN, 3D CNN, and MLP, PHNet effectively captures both local and global features. Additionally, we proposed a permutable MLP block to address spatial information loss and alleviate computational burden. Experimental results on four public datasets demonstrate the superiority of PHNet over state-of-the-art approaches. Future research will explore extending the framework to other medical image analysis tasks, such as disease diagnosis and localization, and further examine the interactions and effectiveness of CNN, Transformer, and MLP.

REFERENCES

- [1] H. Cao, Y. Wang, J. Chen, D. Jiang, X. Zhang, Q. Tian, and M. Wang, "Swin-Unet: UNet-like pure transformer for medical image segmentation," in *European Conference on Computer Vision*, 2023.
- [2] D. Zhang, Y. Lin, H. Chen, Z. Tian, X. Yang, J. Tang, and K. T. Cheng, "Deep learning for medical image segmentation: tricks, challenges and future directions," *arXiv*, 2022.
- [3] J. Chen, Y. Lu, Q. Yu, X. Luo, E. Adeli, Y. Wang, L. Lu, A. L. Yuille, and Y. Zhou, "TransUNet: Transformers make strong encoders for medical image segmentation," *arXiv*, 2021.
- [4] O. Ronneberger, P. Fischer, and T. Brox, "U-Net: Convolutional networks for biomedical image segmentation," in *International Conference on Medical Image Computing and Computer Assisted Intervention*. Springer, 2015, pp. 234–241.
- [5] K. He, X. Zhang, S. Ren, and J. Sun, "Deep residual learning for image recognition," in *Proceedings of the IEEE Conference on Computer Vision and Pattern Recognition*, 2016, pp. 770–778.

- [6] S. Mehta, E. Merca, J. Bartlett, D. Weaver, J. G. Elmore, and L. Shapiro, "Y-Net: joint segmentation and classification for diagnosis of breast biopsy images," in *International Conference on Medical Image Computing and Computer Assisted Intervention*. Springer, 2018, pp. 893–901.
- [7] F. Milletari, N. Navab, and S.-A. Ahmadi, "V-Net: Fully convolutional neural networks for volumetric medical image segmentation," in *International Conference on 3D Vision*. Ieee, 2016, pp. 565–571.
- [8] A. Vaswani, N. Shazeer, N. Parmar, J. Uszkoreit, L. Jones, A. N. Gomez, E. Kaiser, and I. Polosukhin, "Attention is all you need," *Advances in Neural Information Processing Systems*, vol. 30, 2017.
- [9] A. Dosovitskiy, L. Beyer, A. Kolesnikov, D. Weissenborn, X. Zhai, T. Unterthiner, M. Dehghani, M. Minderer, G. Heigold, S. Gelly, J. Uszkoreit, and N. Houlsby, "An image is worth 16x16 words: Transformers for image recognition at scale," *ICLR*, 2021.
- [10] H. Touvron, M. Cord, M. Douze, F. Massa, A. Sablayrolles, and H. Jégou, "Training data-efficient image transformers & distillation through attention," in *International Conference on Machine Learning*. PMLR, 2021, pp. 10347–10357.
- [11] A. Hatamizadeh, Y. Tang, V. Nath, D. Yang, A. Myronenko, B. Landman, H. R. Roth, and D. Xu, "UNETR: Transformers for 3D medical image segmentation," in *Proceedings of the IEEE/CVF Winter Conference on Applications of Computer Vision*, 2022, pp. 574–584.
- [12] Y. Xie, J. Zhang, C. Shen, and Y. Xia, "CoTr: Efficiently bridging cnn and transformer for 3D medical image segmentation," in *International Conference on Medical Image Computing and Computer Assisted Intervention*. Springer, 2021, pp. 171–180.
- [13] J. M. J. Valanarasu and V. M. Patel, "UNeXt: MLP-based rapid medical image segmentation network," in *International Conference on Medical Image Computing and Computer Assisted Intervention*. Springer, 2022, pp. 23–33.
- [14] I. O. Tolstikhin, N. Houlsby, A. Kolesnikov, L. Beyer, X. Zhai, T. Unterthiner, J. Yung, A. Steiner, D. Keysers, J. Uszkoreit *et al.*, "MLP-mixer: An all-MLP architecture for vision," *Advances in Neural Information Processing Systems*, vol. 34, pp. 24261–24272, 2021.
- [15] H. R. Roth, Z. Xu, C. Tor-Díez, R. S. Jacob, J. Zember, J. Molto, W. Li, S. Xu, B. Turkbey, E. Turkbey *et al.*, "Rapid artificial intelligence solutions in a pandemic—the covid-19-20 lung ct lesion segmentation challenge," *Medical Image Analysis*, vol. 82, p. 102605, 2022.
- [16] B. Landman, Z. Xu, J. Igelsias, M. Styner, T. Langerak, and A. Klein, "MiccAI multi-atlas labeling beyond the cranial vault—workshop and challenge," in *Proc. MICCAI Multi-Atlas Labeling Beyond Cranial Vault—Workshop Challenge*, vol. 5, 2015, p. 12.
- [17] Q. Dou, H. Chen, Y. Jin, L. Yu, J. Qin, and P.-A. Heng, "3d deeply supervised network for automatic liver segmentation from ct volumes," in *Medical Image Computing and Computer-Assisted Intervention—MICCAI 2016: 19th International Conference, Athens, Greece, October 17–21, 2016, Proceedings, Part II 19*. Springer, 2016, pp. 149–157.
- [18] S. Liu, D. Xu, S. K. Zhou, O. Pauly, S. Grbic, T. Mertelmeier, J. Wicklein, A. Jerebko, W. Cai, and D. Comaniciu, "3D anisotropic hybrid network: Transferring convolutional features from 2D images to 3D anisotropic volumes," in *International Conference on Medical Image Computing and Computer Assisted Intervention*. Springer, 2018, pp. 851–858.
- [19] T. Falk, D. Mai, R. Bensch, Ö. Çiçek, A. Abdulkadir, Y. Marrakchi, A. Böhm, J. Deubner, Z. Jäckel, K. Seiwald *et al.*, "U-Net: deep learning for cell counting, detection, and morphometry," *Nature Methods*, vol. 16, no. 1, pp. 67–70, 2019.
- [20] Z. Dong, Y. He, X. Qi, Y. Chen, H. Shu, J.-L. Coatrieux, G. Yang, and S. Li, "MNet: Rethinking 2D/3D networks for anisotropic medical image segmentation," in *International Joint Conferences on Artificial Intelligence*, 2022.
- [21] H. Peiris, M. Hayat, Z. Chen, G. Egan, and M. Harandi, "A robust volumetric transformer for accurate 3d tumor segmentation," in *Medical Image Computing and Computer Assisted Intervention—MICCAI 2022: 25th International Conference, Singapore, September 18–22, 2022, Proceedings, Part V*. Springer, 2022, pp. 162–172.
- [22] Y. Tang, D. Yang, W. Li, H. R. Roth, B. Landman, D. Xu, V. Nath, and A. Hatamizadeh, "Self-supervised pre-training of swin transformers for 3D medical image analysis," in *Proceedings of the IEEE Conference on Computer Vision and Pattern Recognition*, 2022, pp. 20730–20740.
- [23] S. Chen, E. Xie, C. GE, R. Chen, D. Liang, and P. Luo, "CycleMLP: A MLP-like architecture for dense prediction," in *International Conference on Learning Representations*, 2022. [Online]. Available: <https://openreview.net/forum?id=NMEceG4v69Y>
- [24] Y. Tang, K. Han, J. Guo, C. Xu, Y. Li, C. Xu, and Y. Wang, "An image patch is a wave: Phase-aware vision MLP," in *Proceedings of the IEEE Conference on Computer Vision and Pattern Recognition*, 2022, pp. 10935–10944.
- [25] P. W. Battaglia, J. B. Hamrick, V. Bapst, A. Sanchez-Gonzalez, V. Zambaldi, M. Malinowski, A. Tacchetti, D. Raposo, A. Santoro, R. Faulkner *et al.*, "Relational inductive biases, deep learning, and graph networks," *arXiv*, 2018.
- [26] G. Wang, J. Shapey, W. Li, R. Dorent, A. Dimitriadis, S. Bisdas, I. Paddick, R. Bradford, S. Zhang, S. Ourselin *et al.*, "Automatic segmentation of vestibular schwannoma from T2-weighted mri by deep spatial attention with hardness-weighted loss," in *International Conference on Medical Image Computing and Computer Assisted Intervention*. Springer, 2019, pp. 264–272.
- [27] D. Ulyanov, A. Vedaldi, and V. Lempitsky, "Instance normalization: The missing ingredient for fast stylization," *arXiv*, 2016.
- [28] Q. Hou, Z. Jiang, L. Yuan, M.-M. Cheng, S. Yan, and J. Feng, "Vision permutator: A permutable MLP-like architecture for visual recognition," *IEEE Transactions on Pattern Analysis and Machine Intelligence*, vol. 45, no. 1, pp. 1328–1334, 2022.
- [29] H. Liu, Z. Dai, D. So, and Q. V. Le, "Pay attention to MLPs," *Advances in Neural Information Processing Systems*, vol. 34, pp. 9204–9215, 2021.
- [30] D. J. Zhang, K. Li, Y. Wang, Y. Chen, S. Chandra, Y. Qiao, L. Liu, and M. Z. Shou, "MorphMLP: An efficient mlp-like backbone for spatial-temporal representation learning," in *European Conference on Computer Vision*. Springer, 2022, pp. 230–248.
- [31] R. Liu, Y. Li, L. Tao, D. Liang, and H.-T. Zheng, "Are we ready for a new paradigm shift? a survey on visual deep MLP," *Patterns*, vol. 3, no. 7, p. 100520, 2022.
- [32] F. Wang, M. Jiang, C. Qian, S. Yang, C. Li, H. Zhang, X. Wang, and X. Tang, "Residual attention network for image classification," in *Proceedings of the IEEE Conference on Computer Vision and Pattern Recognition*, 2017, pp. 3156–3164.
- [33] F. Zhang, Y. Wang, and H. Yang, "Efficient context-aware network for abdominal multi-organ segmentation," *arXiv*, 2021.
- [34] M. J. Cardoso, W. Li, R. Brown, N. Ma, E. Kerfoot, Y. Wang, B. Murrey, A. Myronenko, C. Zhao, D. Yang *et al.*, "Monai: An open-source framework for deep learning in healthcare," *arXiv*, 2022.
- [35] I. Loshchilov and F. Hutter, "Decoupled weight decay regularization," in *International Conference on Learning Representations*, 2019.
- [36] F. Isensee, P. F. Jaeger, S. A. Kohl, J. Petersen, and K. H. Maier-Hein, "nnU-Net: a self-configuring method for deep learning-based biomedical image segmentation," *Nature Methods*, vol. 18, no. 2, pp. 203–211, 2021.
- [37] J. Schlemper, O. Oktay, M. Schaap, M. Heinrich, B. Kainz, B. Glocker, and D. Rueckert, "Attention gated networks: Learning to leverage salient regions in medical images," *Medical Image Analysis*, vol. 53, pp. 197–207, 2019.
- [38] Y. Lin, D. Zhang, X. Fang, Y. Chen, K.-T. Cheng, and H. Chen, "Rethinking boundary detection in deep learning models for medical image segmentation," in *International Conference on Information Processing in Medical Imaging*, 2023.
- [39] D. Lian, Z. Yu, X. Sun, and S. Gao, "As-mlp: An axial shifted mlp architecture for vision," in *International Conference on Learning Representations (ICLR)*, 2022.
- [40] K. Zhang and D. Liu, "Customized segment anything model for medical image segmentation," *arXiv*, 2023.
- [41] A. Kirillov, E. Mintun, N. Ravi, H. Mao, C. Rolland, L. Gustafson, T. Xiao, S. Whitehead, A. C. Berg, W.-Y. Lo *et al.*, "Segment anything," *arXiv*, 2023.
- [42] E. J. Hu, P. Wallis, Z. Allen-Zhu, Y. Li, S. Wang, L. Wang, W. Chen *et al.*, "Lora: Low-rank adaptation of large language models," in *International Conference on Learning Representations*, 2021.
- [43] P. Bilic, P. Christ, H. B. Li, E. Vorontsov, A. Ben-Cohen, G. Kaissis, A. Szeskin, C. Jacobs, G. E. H. Mamani, G. Chartrand *et al.*, "The liver tumor segmentation benchmark (lits)," *Medical Image Analysis*, vol. 84, p. 102680, 2023.
- [44] M. Antonelli, A. Reinke, S. Bakas, K. Farahani, A. Kopp-Schneider, B. A. Landman, G. Litjens, B. Menze, O. Ronneberger, R. M. Summers *et al.*, "The medical segmentation decathlon," *Nature communications*, vol. 13, no. 1, p. 4128, 2022.
- [45] G. Bertasius, H. Wang, and L. Torresani, "Is space-time attention all you need for video understanding?" in *ICML*, vol. 2, no. 3, 2021, p. 4.